Kobe University Repository : Kernel

PDF issue: 2025-12-05

Formation mechanism of ferroelectric poly (vinylidene fluoride-trifluoroethylene) copolymers with in-plane dipole alignment under low electric field from melt and its SPR based…

Sutani, Yohei
Koshiba, Yasuko
Fukushima, Tatsuya
Ishida, Kenji

(Citation)
Polymer,228:123904

(Issue Date)
2021-07-16

(Resource Type)
journal article

(Version)
Version of Record

(Rights)
© 2021 The Authors. Published by Elsevier Ltd.
This is an open access article under the CC BY license
(http://creativecommons.org/licenses/by/4.0/).

(URL)
https://hdl.handle.net/20.500.14094/90008460

Polymer 228 (2021) 123904

Contents lists available at ScienceDirect

Polymer

journal homepage: www.elsevier.com/locate/polymer

Formation mechanism of ferroelectric poly (vinylidene fluoride-trifluoroethylene) copolymers with in-plane dipole alignment under low electric field from melt and its SPR based pyroelectric sensor

Yohei Sutani, Yasuko Koshiba, Tatsuya Fukushima, Kenji Ishida *

Department of Chemical Science and Engineering, Graduate School of Engineering, Kobe University, 1-1, Rokkodai-cho, Nada-ku, Kobe, Hyogo, 657-8501, Japan

ARTICLE INFO

Keywords:
In-plane dipole alignment
Pyroelectric properties
Surface plasmon resonance

ABSTRACT

P(VDF/TrFE) thin films were annealed under a low electric field using microgapped comb-like electrodes (IDT structure), and their structures and pyroelectric properties were investigated. In-plane dipole alignment of P(VDF/TrFE) was achieved by applying a low electric field (7.7 MV m^{-1}), and the I phase crystal structure with in-plane dipole alignment was transformed following nucleation of the III phase structure. Despite the absence of a Fabry–Perot-type infrared absorption structure, the P(VDF/TrFE) thin films, which were continuously subjected to a low electric field from the melting point to para-ferroelectric phase transition temperature, exhibited a large pyroelectric signal. The voltage sensitivity was 242 V W^{-1}, which is much higher than that of the sandwich type sensor equipped with a Fabry–Perot-type infrared absorption structure on Si substrates (72 V W^{-1}). The improved sensitivity could be attributed to the suppression of the injected charges under the application of a low electric field and the enhancement of the infrared absorption and infrared-to-thermal conversion owing to the surface plasmon resonance on the microgapped IDT structure.

1. Introduction

Infrared sensors can detect infrared rays emitted by people and objects. In addition to conventional applications, such as crime prevention, and medical and infectious disease countermeasures, sensors installed in air conditioners can detect people and improve energy efficiency while providing comfort [1]. Sensors installed in cars can identify people and vehicles in any environment, thus preventing accidents and assisting in autonomous and advanced driving [2]. The applications of infrared sensors have become more diverse.

Pyroelectric infrared sensors have advantages over semiconductor-based sensors in that they can be used uncooled and have a wide range of selectivity in the infrared wavelengths to be detected. Currently, the materials used for pyroelectric infrared sensors are inorganic ferroelectrics such as lead zirconate titanate (PZT) and lithium tantalate. Inorganic ferroelectrics exhibit excellent pyroelectric properties and can be applied to microintegration processes [3–6]. However, in terms of the environment and sustainability of material supply, they have disadvantages, such as the inclusion of lead, which is regulated by the RoHS directive, and minor metals that are rarely distributed. Therefore, organic ferroelectrics are attracting attention as alternatives to inorganic ferroelectrics.

Vinylidene fluoride (-CH_2CF_2-; VDF)-based materials have an electric dipole moment (2.1 D) perpendicular to the molecular chain, resulting from the difference in the electronegativities between the hydrogen and fluorine atoms in the monomer unit. VDF-based materials with well controlled electric dipoles exhibit higher ferroelectricity (P_r: 130 mC m^{-2}) and pyroelectricity values than general-purpose organic materials ($|\rho|$: 68 μC m^{-2} K^{-1}) [7–9]. Poly (vinylidene fluoride-trifluoroethylene) copolymers [P(VDF/TrFE)] have been widely studied owing to its ability to form stable ferroelectric crystal structure (I or β phase) films through simple melt-solidification, casting, and spin coating. We previously reported that it is possible to fabricate sensors with good pyroelectric properties using P(VDF/TrFE) freestanding films [10].

VDF-based materials typically have three types of crystal structures [11,12]: a I phase crystal structure (all-*trans* conformation and parallel packing) with the highest ferroelectricity, a II phase structure (α phase: *TGTG′* and anti-parallel packing) with no ferroelectricity, and a III phase structure (γ phase: T_3GT_3G' and parallel packing) with approximately 64% of the I phase ferroelectricity. The degree of pyroelectricity is improved with the increase in the proportion of ferroelectric crystal phases, such as in the I phase crystal structure. In addition to the

* Corresponding author.
E-mail address: kishida@crystal.kobe-u.ac.jp (K. Ishida).

https://doi.org/10.1016/j.polymer.2021.123904
Received 5 March 2021; Received in revised form 22 May 2021; Accepted 22 May 2021
Available online 26 May 2021
0032-3861/© 2021 The Authors. Published by Elsevier Ltd. This is an open access article under the CC BY license (http://creativecommons.org/licenses/by/4.0/).

ferroelectric crystal structure, it is important to control the polarization arrangement in one direction to develop pyroelectricity, and the crystal structure and polarization control can be realized by applying an electric field after film formation. Because the polarization alignment of P(VDF/TrFE) is controlled by the rotation of the molecular chains, the high electric field required to control the polarization is more than 10 times that in the case of the PZT, in which the polarization is spontaneous because of the arrangement of positive and negative ions (PZT: ~5 MV m^{-1}, P(VDF/TrFE): ~100 MV m^{-1}) [13,14]. We previously reported that in low-molecular-weight VDF oligomers, charge is injected into the thin film via polarization control by applying a high electric field, resulting in a significant difference in the pyroelectric properties [15]. Therefore, to avoid dielectric breakdown and deterioration of the pyroelectric sensor's performance from the high electric field, a method of polarization control with a low electric field is essential.

In this study, a low electric field (7.7 MV m^{-1}) was applied during crystallization of P(VDF/TrFE) from the melt. To discuss the mechanism of formation of the ferroelectric I phase crystal structure and polarization alignment under the low electric field, we performed structural characterization during the annealing process under the low electric field. Studies have reported ferroelectric-to-paraelectric transition and structural changes in VDF-based materials under electric field application during heating; however, in those cases, the electric field applied exceeded the electric field at which polarization reversal occurs (coercive electric field; E_c) [16,17]. Notably, in the present study, the crystal structure and polarization alignment were controlled by applying an electric field lower than E_c during heating. It is difficult to apply an electric field during the annealing process in a typical sandwich structure. This is because at temperatures above the melting point, the P(VDF/TrFE) melts and softens, which results in the sandwich structures being easily destroyed and an electrical short circuit occurring between the top and bottom electrodes. In this study, we fabricated sensors using a microgapped comb-like electrode (IDT) structure for electric field application during annealing, and evaluated their pyroelectric properties.

2. Experimental

2.1. Materials

P(VDF/TrFE) (Fig. 1(a)) was purchased from KUREHA (VDF/TrFE molar ratio of 75/25, M_w = 350,000). Methyl ethyl ketone (MEK) was purchased from Nacalai Tesque.

2.2. Microgapped IDT structure fabrication

A 5 nm thick Cr and a 50 nm thick Au layer were deposited on a SiO_2/Si wafer by vacuum evaporation. Laser lithography and subsequent wet etching were performed to pattern the microgapped IDT (Fig. 1(b)). The distance between the electrodes was set to 1.3 μm, the electrode width to 2.0 μm, and the pitch to 6.6 μm.

2.3. Film formation by applying a low electric field

P(VDF/TrFE) powder was dissolved in the MEK. Thin films of P(VDF/TrFE) were deposited on the IDT structure by spin coating. After solvent drying, the film thickness was 100 nm, as measured by a stylus profiler (Fig. 1(c)). A DC electric field of 7.7 MV m^{-1} (10 V) was applied between the electrodes during heating at 438 K and cooling in a vacuum chamber (5×10^{-4} Pa).

2.4. Differential scanning calorimetry (DSC)

The thermal properties were evaluated by DSC to determine the annealing temperature required for the crystallization of P(VDF/TrFE) thin films. DSC measurements were carried out at a scanning speed of 10 K min^{-1} under atmospheric conditions.

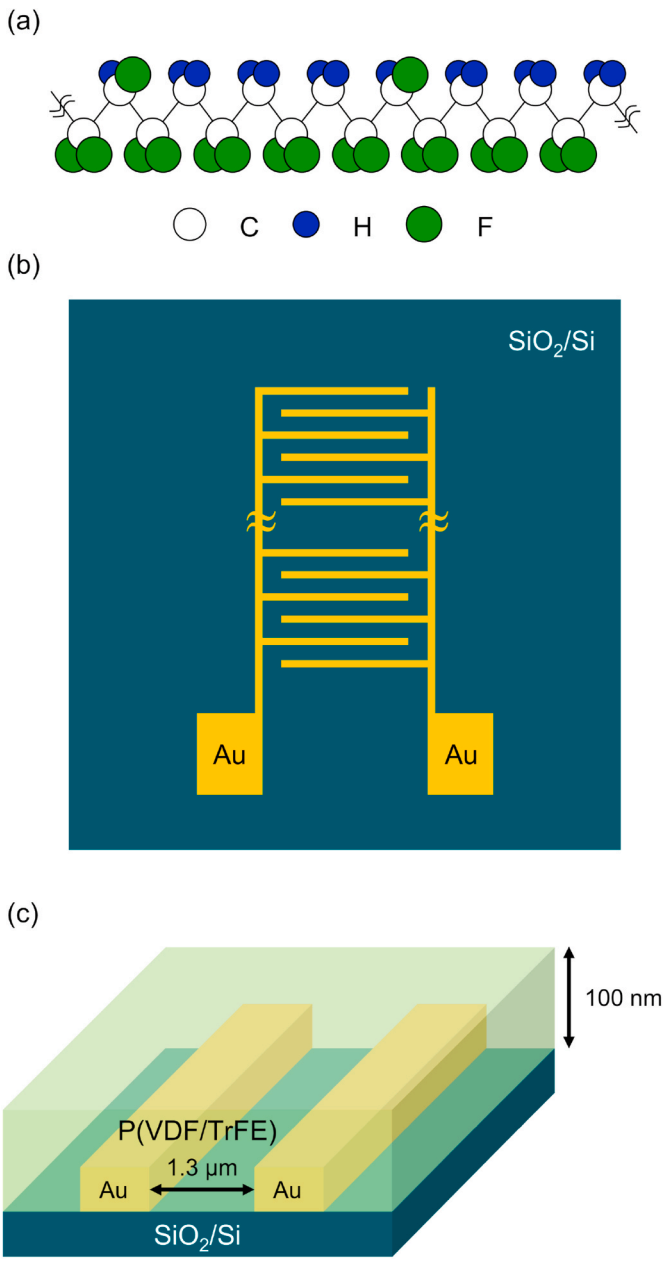

Fig. 1. (a) Schematic image of chemical structure of the P(VDF/TrFE), (b) schematic of comb-like (IDT) electrodes fabricated on a SiO_2/Si substrate, and (c) oblique drawing of our pyroelectric sensor structure.

2.5. Current density (J)–Electric field (E) switching curve measurement

The *J–E* switching curve is the change in current density when an AC electric field is applied, and its current peak indicates charge-discharge associated with polarization reversal. The peak position is the electric field required for polarization control (coercive electric field: E_c). In this study, a triangular wave electric field is applied and the frequency is 10 Hz under atmospheric conditions.

2.6. Fourier transform infrared (FT-IR) spectroscopy

The molecular conformation and orientation were analyzed by FT-IR spectroscopy (JASCO, FT/IR-6600, and IRT-5200) in the transmission mode. To discuss the structural changes during heating and cooling,

temperature change interval measurements were carried out using a microscope cooling and heating stage (Japan High Tech, Linkam 10002).

2.7. Pyroelectric characteristic measurement

To characterize the pyroelectric sensor, a blackbody source was used to generate infrared radiation. The pyroelectric current generated by the infrared incidence was amplified and converted into voltage using a voltage follower circuit, and the output voltage was monitored using an oscilloscope (Tektronix, Inc. TDS5034B). To calculate the voltage sensitivity, the frequency components were extracted from the output voltage using a lock-in amplifier (NF Corporation, LI5640), and the incident infrared energy was measured using a power meter. In this study, the blackbody furnace temperature was 773 K, and the chopping frequency was set to values ranging from 0.2 to 200 Hz using a mechanical chopper. Because the infrared irradiated area and electrode area are different in the IDT structure, the area between the gaps, where P(VDF/TrFE) is irradiated with infrared rays and pyroelectric current can be extracted, was used to calculate the voltage sensitivity. To evaluate the effect of the high electric field applied after film formation on the pyroelectric properties, a ferroelectric evaluation system (TOYO, FEC-1, Japan) was used to perform polarization treatments based on the application of a triangular wave voltage.

3. Results and discussion

3.1. DSC and J–E switching curve of P(VDF/TrFE)

Fig. 2 shows the DSC curve of P(VDF/TrFE). Four peaks can be identified, two during the heating process and two during the cooling process. The peak at 393 K during the heating process is the Curie point during the temperature rise ($T_{Curie\ 1}$) and the peak at 426 K is the melting point (T_{melt}). The peak at 400 K during the cooling process is the crystallization temperature ($T_{crystallization}$) and the peak at 342 K is the Curie point during the temperature drop ($T_{Curie\ 2}$). Curie points of P(VDF/TrFE) are different when the temperature rises and falls. This is because the ferroelectric-paraelectric phase transition of P(VDF/TrFE) is a first order phase transition with latent heat [18]. The typical crystallization annealing temperature for P(VDF/TrFE) was set between $T_{Curie\ 1}$ and T_{melt} (in our study, we set it to 403 K) [19]; however, in this experiment, the annealing temperature was set to 438 K, which is above T_{melt} because the application of an electric field in a high molecular mobility state is considered effective. Ohigashi et al. reported that the cooling process is important for the single crystallization of P(VDF/TrFE) [20], and the pyroelectric properties were observed when the electric field was applied even during cooling in corona poling during the annealing process [21]; therefore, the cooling process in which the crystal structure is formed is considered important. As such, in this study, a low electric field was applied from 373 K during the heating process through 438 K to 333 K during the cooling process, i.e., the melting, crystallization, and ferroelectric phase transition regions, as shown in Fig. 2.

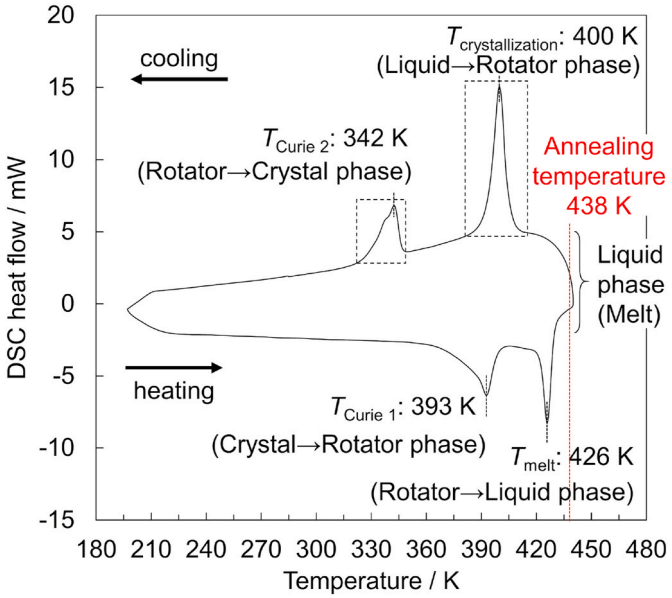

Fig. 2. DSC curve of P(VDF/TrFE).

Fig. 3 shows the *J–E* switching curve of the P(VDF/TrFE) thin film in a typical sandwich structure. A peak due to polarization reversal (E_c) can be observed at 53 MV m^{-1}. The applied electric field in this experiment was 7.7 MV m^{-1}, which is extremely low compared to E_c. Notably, polarization control is typically not possible at this electric field magnitude.

3.2. FT-IR absorption spectra and dipole alignment model of P(VDF/TrFE) thin films annealed with low electric field

Fig. 4 shows the FT-IR transmission spectra of the P(VDF/TrFE) thin films with only solvent drying (as-spun), annealed without an electric field, and annealed with a low electric field. The assignment of each infrared absorption band was based on the FT-IR spectrum of PVDF—which has the same main-chain structure and has been theoretically calculated [22–25]—and P(VDF/TrFE), which has been reported [26,27]. The baseline rising up at the lower wavenumber can be attributed to the interference due to the film thickness. The as-spun films exhibited four peaks attributed to crystals and amorphous CH_2 symmetric stretching vibration [$\nu_s(CH_2)$] and CH_2 antisymmetric stretching vibration [$\nu_a(CH_2)$], whereas the films annealed without an applied electric field gave two peaks attributed to the I phase crystal structures of $\nu_s(CH_2)$ and $\nu_a(CH_2)$. This indicates that the annealing process accelerated crystallization. On the other hand, six peaks were observed in the film when a low electric field was applied during the annealing process. Because the peak splits in the CH_2 stretching region in the III phase crystal structure of PVDF [23], it is presumed that the newly appeared peak due to the application of a low electric field is the peak due to the ferroelectric III phase crystal structure. In addition, the peak intensity of the I phase crystalline phase with the highest ferroelectricity is increased. Therefore, the application of an electric field as low as 7.7 MV m^{-1} during the annealing was found to cause structural induction to

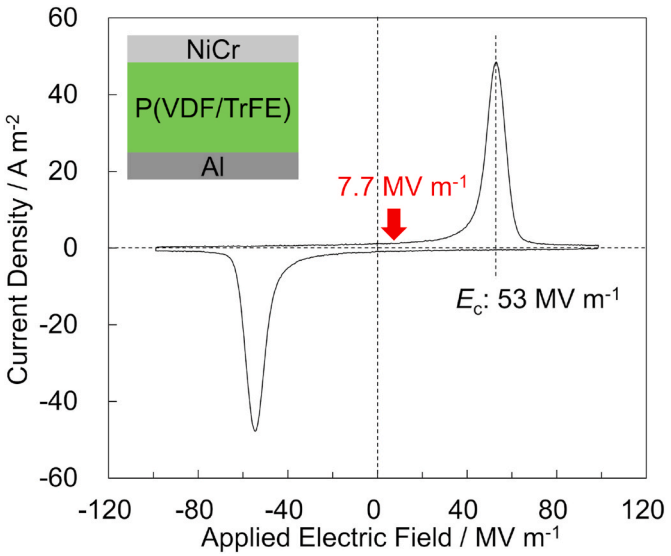

Fig. 3. *J–E* switching curve of P(VDF/TrFE) in the sandwich structure.

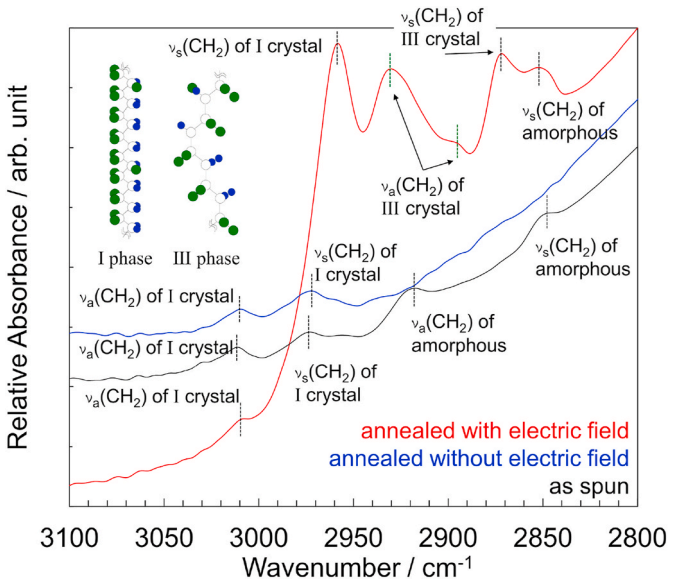

Fig. 4. FT-IR transmission absorption spectra of as-spun, annealed without electric field, and annealed with electric field P(VDF/TrFE) thin films.

the ferroelectric I and III crystalline phase.

Assuming that the ferroelectric crystal structure is formed by the electrostatic interaction between the electric dipole of P(VDF/TrFE) and the applied low electric field in the in-plane direction of the substrate, two possible structure models will be considered, as shown in Fig. 5. Fig. 5(a) shows the model where the molecular chains are oriented parallel to the substrate. Fig. 5(b) shows the model where this orientation is perpendicular. When the molecular chains are oriented in parallel, the transition moment of $\nu_s(CH_2)$ is in the in-plane direction to the substrate, and the transition moment of $\nu_a(CH_2)$ is out-of-plane. On the other hand, when the molecular chains are oriented perpendicularly, the transition moment of $\nu_s(CH_2)$ and $\nu_a(CH_2)$ is in the in-plane direction. The FT-IR transmission method strongly detects the transition moment in the in-plane direction of the substrate. In the spectrum shown in Fig. 4, $\nu_s(CH_2)$ is strongly and $\nu_a(CH_2)$ is weakly detected, so the molecular chain is presumed to be oriented parallel to the substrate, and the model in Fig. 5(a) is considered correct. Even if the molecular chains are oriented in parallel, the $\nu_s(CH_2)$ and $\nu_a(CH_2)$ peak intensities will not be anisotropic if the polarization alignment is not controlled. In fact, there is no anisotropy in the spectrum of the thin film without an electric field during the annealing process. Therefore, the in-plane polarization of P(VDF/TrFE) could be controlled by applying the low electric field of only 7.7 MV m^{-1} during the annealing process.

To analyze the formation process of the ferroelectric P(VDF/TrFE) crystal with in-plane polarization under the low electric field, FT-IR interval measurements were conducted during the cooling process. Fig. 6 shows the temperature dependence of the transmission FT-IR spectrum. An absorption peak was observed at 438 K in the melt state in Fig. 6(a) and (b). This indicates that the molecular chain conformation of P(VDF/TrFE) exists near the melting point, although there is no molecular packing as a crystal structure. In the past, the similar absorption peak has been reported to be obtained by heating above the melting point of P(VDF/TrFE) [28]. In the P(VDF/TrFE) thin film annealed without an applied electric field (Fig. 6(a)), the peak around 1190 cm^{-1} [CF_2 antisymmetric stretching vibration ($\nu_a(CF_2)$) of the *TGTG′* structure] increased at 413 K, and the peak around 1400 cm^{-1} [CH_2 wagging vibration ($w(CH_2)$) of the *TGTG′* structure] decreased during the cooling process. Since a temperature of 413 K corresponds to the start of the crystallization region in the DSC curve shown in Fig. 2, it is believed that P(VDF/TrFE), which was in the *TGTG′* structure in the melt region, became more ordered and started to pack in the lattice points of hexagonal phase. In references [29] and [30], it has been reported that the P(VDF/TrFE) molecule transitions to the rotational phase, where the molecular chain rotates at the lattice points of hexagonal phase during the cooling process. In this paper, we describe this state as "rotator phase with *TGTG′* structure." With further cooling, at 342 K, the peak near 1190 cm^{-1} shifted to a lower wavenumber, the peak at 1290 cm^{-1} appeared, and the peaks near 1400 cm^{-1} and 1430 cm^{-1} shifted to higher wavenumbers. This shows the shift of $\nu_a(CF_2)$ from the rotator phase with *TGTG′* structure to I phase crystal structure, the appearance of CF_2 symmetric stretching vibration [$\nu_s(CF_2)$] in the I phase, and the shift of the $w(CH_2)$ and CH_2 bending vibrations [$\delta(CH_2)$] from the rotator phase with *TGTG′* structure to I phase. As a temperature of 342 K is $T_{Curie\ 2}$ in the DSC curve, the transition from the rotator phase with *TGTG′* structure to I phase is considered to occur in the ferroelectric phase transition region. Fig. 7(a) shows the crystal formation model during the cooling process of the thin film without applying an electric field during the annealing process. In the melt region, the molecules of the *TGTG′* structure are in a state of free movement. As cooling proceeds, the translational motion of the molecular chains is restricted in the crystallization region, resulting in the packing of the lattice points of hexagonal phase. In this region, the structure was not completely fixed, but the structure of P(VDF/TrFE) is presumed to be rotator phase. As the cooling progresses further, the rotational motion of the molecular chains becomes weak, and the structure transitions to the I phase crystal structure. At this time, the molecular chain structure transitions from the *TGTG′* structure to the all-*trans* structure, and the crystal structure transitions from hexagonal phase to orthorhombic. Even if an I phase structure is formed, the polarization arrangement is random; thus, pyroelectricity does not develop.

In the P(VDF/TrFE) thin film annealed under an applied low electric field (Fig. 6(b)), the $\nu_a(CF_2)$ peak in the T_3GT_3G' structure is located around 1240 cm^{-1} in the melt region at 438 K; thus, the T_3GT_3G' structure is included by applying a low electric field. However, the peak at around 1430 cm^{-1} [$\delta(CH_2)$] and the broad peak at around 1190 cm^{-1} [$\nu_a(CF_2)$] indicate the presence of a *TGTG′* structure. P(VDF/TrFE) melt is presumed to be a mixture of *TGTG′* structure and field-induced T_3GT_3G' structure. When cooled to 433 K, the broad peak at 1190 cm^{-1} became a sharp peak. The *TGTG′* structure was transferred to the T_3GT_3G' structure by the low electric field with the decreasing temperature. As the cooling proceeded to 413 K, the peak around 1190 cm^{-1}

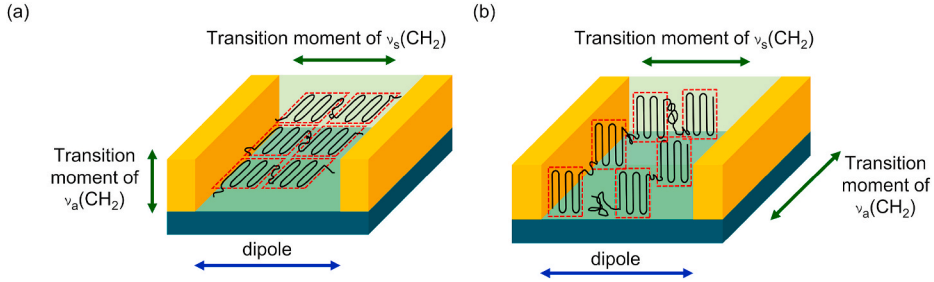

Fig. 5. Dipole alignment model of P(VDF/TrFE); molecular chain orientation is (a) parallel and (b) perpendicular to the substrate.

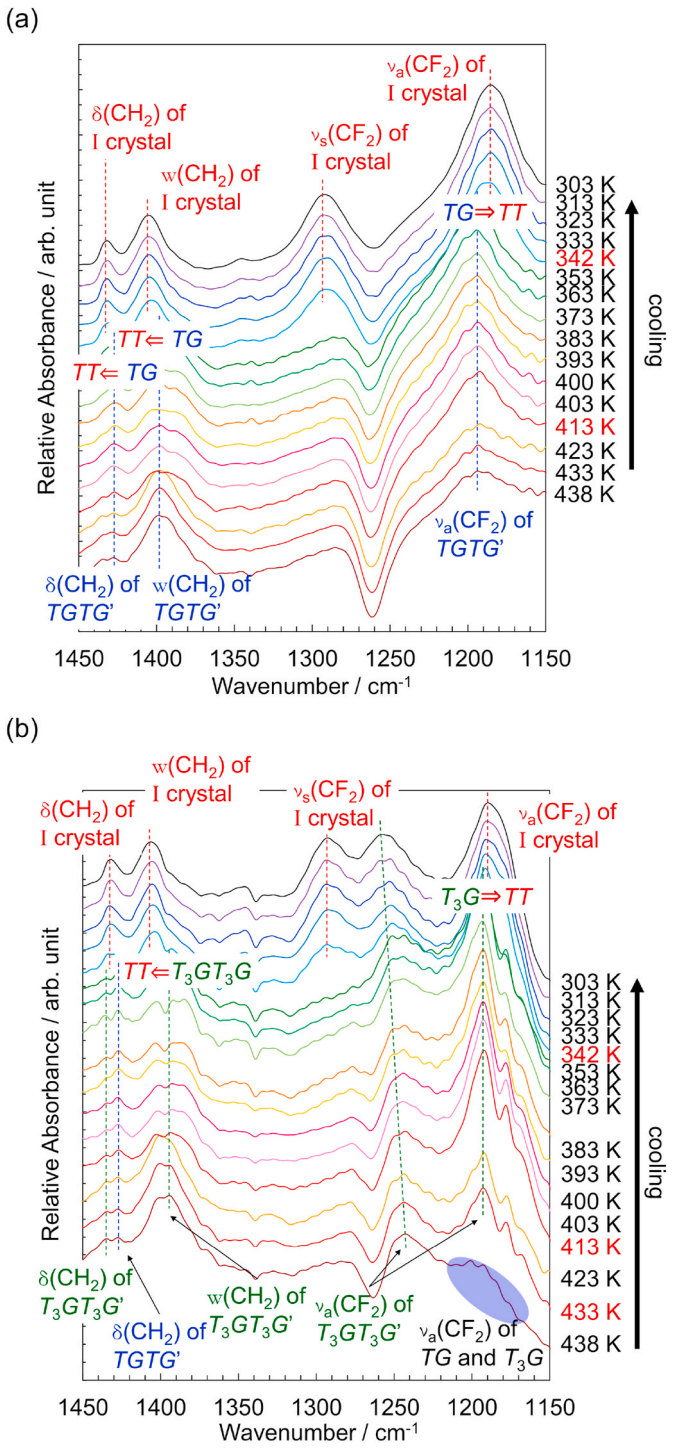

Fig. 6. Temperature dependence of FT-IR transmission absorption spectra during cooling process of (a) annealed without electric field, and (b) annealed with electric field P(VDF/TrFE) thin films.

[($\nu_a(CF_2)$) of the T_3GT_3G' structure] increased, and the peak around 1400 cm^{-1} [$w(CH_2)$ of the T_3GT_3G' structure] decreased. The changes at 413 K are similar to those without an applied electric field, and it is assumed that the P(VDF/TrFE) with the T_3GT_3G' structure in the melt region becomes ordered and starts to pack into the lattice points. In this region, the P(VDF/TrFE) molecular chains are considered to be rotating as well as without the applied the electric field. In this paper, we describe this state as "rotator phase with T_3GT_3G' structure" due to the application of low electric field during recrystallization. With further cooling, at 342 K, (1) the peak near 1190 cm^{-1} shifted to a lower wavenumber, (2) the peak at 1290 cm^{-1} appeared, (3) the peaks near 1400 cm^{-1} shifted to higher wavenumbers, and (4) the peak was reduced to a single peak at 1430 cm^{-1}. This shows the shift of $\nu_a(CF_2)$ from the rotator phase with T_3GT_3G' structure to I phase crystal structure, the appearance of $\nu_s(CF_2)$ in the I phase, the shift of $w(CH_2)$ from the rotator phase with T_3GT_3G' structure to I phase crystal structure, and shift of $\delta(CH_2)$ from the rotator phase with $TGTG'$ structure and the rotator phase with T_3GT_3G' structure to I phase crystal structure. Thus, the transition from the rotator phase with T_3GT_3G' structure to I phase is considered to occur from the paraelectric to the ferroelectric phase transition region at 342 K. Fig. 7(b) shows the crystal formation model during the cooling process of the thin film under the application of a low electric field. In the melt region at 438 K, molecules with a $TGTG'$ structure and an electric field-induced T_3GT_3G' structure are mixed and presumed to be in a free motion state. As cooling proceeds to 433 K in the melt state, the T_3GT_3G' structure is presumed to become stable, overcoming the competition with the $TGTG'$ structure under the low electric field. As cooling proceeds at 413 K, the translational motion of the molecular chains is restricted in the crystallization region, resulting in the packing of the lattice points. In this region, there is rotational motion of the molecular chains, and the molecular structure is not completely fixed. It is also presumed that the alignment of the P(VDF/TrFE) unit cell is induced so that the polarization axis is oriented in-plane of the substrate under the low electric field. As further cooling progresses (below 342 K), the rotational motion of the molecular chains becomes weak; at this time, the molecular chain structure change from the T_3GT_3G' to the all-*trans* structure, and the crystal structure transits to orthorhombic phase. Furthermore, it is considered that the ferroelectric I phase structure with in-plane dipole alignment was obtained because the crystal structure transitions while maintaining the alignment of the unit cell of the rotational phase. Fig. 8 shows the AFM phase image of the fabricated P(VDF/TrFE) thin film and the possible structural models of its microstructure. The smooth surface morphology without microstructure was observed in the as spun film, as shown in Fig. 8(a). Some holes in the image are expected to formed with evaporating the solvents. It is assumed that the P(VDF/TrFE) thin film is amorphous in conjunction with the results in Fig. 4, as shown in Fig. 8(d). By the annealing, the surface microstructures were observed in Fig. 9(b). The lamellar structure of P(VDF/TrFE) formed by the thermal treatment of 438 K, however, the orientation of the microstructure could not be confirmed (Fig. 8 (e)). On the other hand, the tendency of lamellar orientation to be aligned into the direction of applied electric field has been clearly observed in the thin film annealed with electric field, as shown in Fig. 8 (c). The lamellar structure oriented to the electric field direction (Fig. 8 (f)).

From these experimental results, the application of a low electric field of only 7.7 MV m^{-1} during the annealing process suggested that the rotator phase with T_3GT_3G' structure—similar to the nucleus of the III phase structure—was first formed, followed by the dipole-aligned I phase crystal. Therefore, pyroelectricity is expected without post-poling treatment by a high electric field.

3.3. *Pyroelectric characteristics and infrared-to-thermal conversion model in the microgapped IDT structure*

Fig. 9(a) shows the time variation of the pyroelectric output voltage of the P(VDF/TrFE) thin-film sensors when the infrared rays are irradiated by a chopping frequency of 0.2 Hz. The output voltage immediately increased when the sensor was irradiated with infrared light, and then gradually decreased toward 0 V. By contrast, the output voltage immediately dropped and then gradually increased toward 0 V when the infrared radiation applied to the sensor was stopped. The output signal reverses in the ON/OFF state of the infrared radiation, and the signal increases immediately after the infrared radiation is turned ON/OFF and then decreases; this behavior is typical of pyroelectric sensors that detect

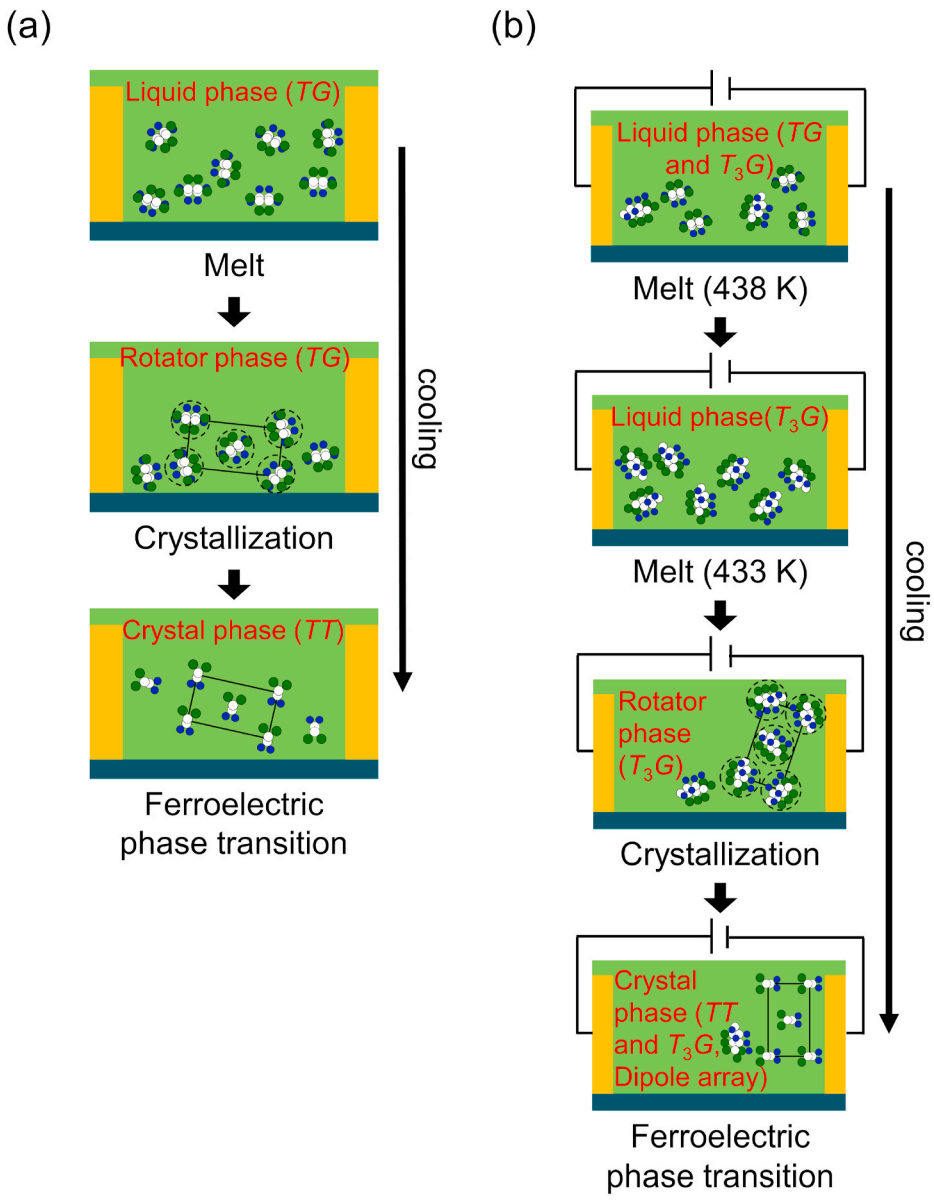

Fig. 7. Overview of solidification during cooling process of (a) annealed without electric field and (b) annealed with electric field P(VDF/TrFE) thin films.

infrared radiation based on the time differentiation of the temperature change. The P(VDF/TrFE) thin films without an electric field applied during the annealing process showed slight pyroelectricity; this may be attributed to the effect of polarization domains near the electrode, as it has been reported that a domain structure different from the bulk structure is formed at the metal interface in ferroelectrics [31]. However, as there was no polarization treatment, a high degree of pyroelectricity could not be obtained. A clear pyroelectric response was observed in the sensor to which a low electric field was applied during the annealing process, and a larger response signal was obtained at an annealing temperature of 438 K compared with that obtained at the typical annealing temperature of 403 K. This indicates that the molecular mobility is insufficient at typical annealing temperatures and that the response to electric fields is low. Heating above T_{melt} resulted in a translational motion in addition to the rotational motion of the molecular chain, the mobility of the molecular chains became extremely high, and the electric field response of the P(VDF/TrFE) molecules is considered to have improved. Therefore, it was assumed that it is important to apply a low electric field in this state.

Fig. 9(b) shows the time variation of the pyroelectric output voltage of the P(VDF/TrFE) thin film sensors before and after polarization treatments under the application of a high electric field (generally called poling treatment). The application of a high electric field after film formation resulted in a significant decrease in the pyroelectric signal. This is consistent with our previous report [15], and it is considered that the application of a high electric field after film formation causes charge injection from the electrode into the films, which inhibits the change in the amount of spontaneous polarization, which is the origin of pyroelectricity. Therefore, to fabricate highly sensitive pyroelectric sensors, controlling the polarization by applying a low electric field during the annealing process is an extremely useful technique.

We focused on the magnitude of the pyroelectric signal shown in Fig. 9. This is because there is a difference in the infrared absorption between the sandwich structure and the IDT structure, as shown in Fig. 10. As shown in Fig. 10(a), in the conventional sandwich structure, infrared-to-thermal conversion is done by infrared absorption using the Fabry–Perot structure [32–37]. By sandwiching the pyroelectric material between NiCr electrodes that transmit and absorb infrared rays [34–36,38] and Al electrodes that reflect infrared rays, we fabricated the Fabry–Perot structure that absorbs infrared rays while repeatedly

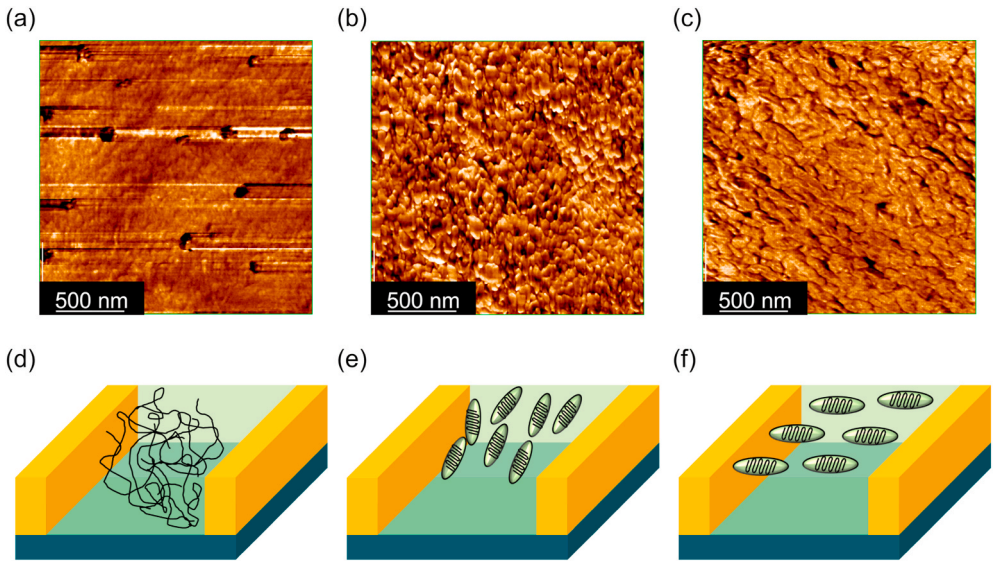

Fig. 8. AFM phase images and the possible structural models of the fabricated P(VDF/TrFE) thin films; (a)(d) as spun, (b)(e) annealed without electric field, and (c)(f) annealed with electric field.

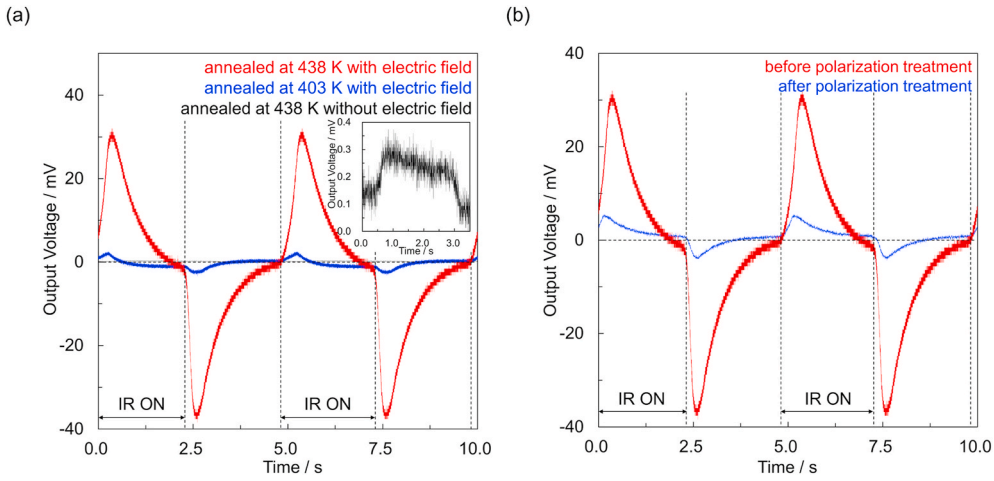

Fig. 9. (a) Output voltage of P(VDF/TrFE) thin films annealed at 403 K and 438 K with electric field, and annealed at 438 K without electric field, and (b) output voltage of P(VDF-TrFE) thin film before and after polarization treatment by applying a high electric field.

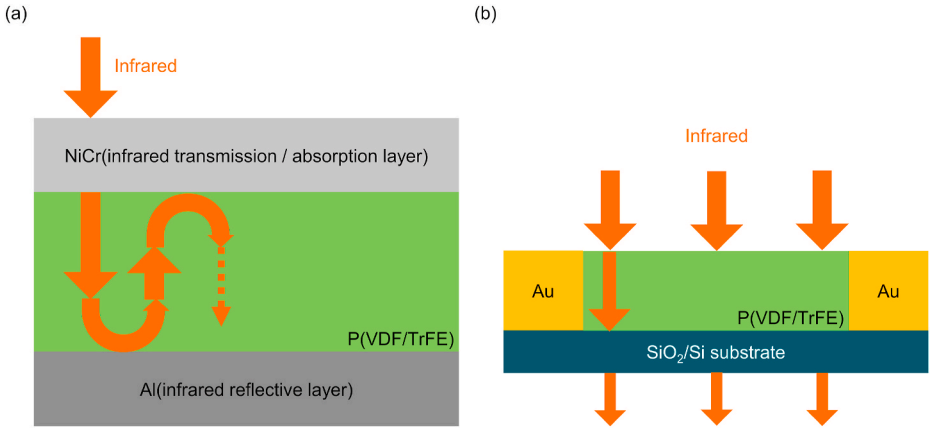

Fig. 10. Model diagram of infrared absorption in (a) sandwich structure and (b) IDT structure.

reflecting them, i.e., a structure that can store infrared rays. This improved the sensor sensitivity of the sandwich structure. While, there is no physical structure in which the incident IR light is repeatedly transmitted and reflected, and the Fabry–Perot condition is not satisfied in the IDT structure, as shown in Fig. 10(b). The incident infrared rays into the IDT structure are only pass through the SiO_2/Si substrate. However, we must note here that the pyroelectric signals on the order of 10 mV were obtained using the microgapped IDT structure. This fact indicates that something new is happening on the microgapped IDT structure. Therefore, we further investigated the infrared absorption in the microgapped IDT structure to identify the factors that lead to large pyroelectric signals.

Fig. 11(a) shows the FT-IR transmission spectra of the P(VDF/TrFE) thin film fabricated on the microgapped IDT structure and Si substrate. The intensity of the absorption peak of the P(VDF/TrFE) thin film on the microgapped IDT structure was observed to be higher than that on the Si substrate. Usually, it is difficult to evaluate an organic thin film with a thickness of approximately 100 nm using the FT-IR transmission method, and it is necessary to use an amplifier to increase the sensitivity; however, in this experiment, no amplifier was used. In addition, the measurement area is smaller in the IDT structure because only the P(VDF/TrFE) existing between the gaps was measured, and the P(VDF/TrFE) on the electrodes could not be measured. Therefore, an extremely high absorption enhancement occurred in the IDT structure. We assume that this phenomenon shows the same behavior as surface-enhanced infrared absorption spectroscopy (SEIRAS) [39,40] and surface-enhanced Raman scattering (SERS) [41]. In SEIRAS and SERS, by using ultrathin metal films and microstructures, the absorption due to molecular vibrations is observed to be much higher than normally obtained. Surface plasmon resonance (SPR) is currently the most promising enhancement mechanism for SEIRAS and SERS. SPR is well-known for enhancing the optical absorption by employing metallic microstructures of sub-wavelength size and for controlling the absorption wavelength by controlling the microstructure [42,43]. In SPR in the infrared region, it is considered that the high efficiency of the absorbed infrared radiation is converted into heat. Since the usefulness of SPR in bolometers, a type of infrared sensor, has been reported [44], more research is being conducted on the application of SPR to infrared sensors [45,46]. Furthermore, the structural parameter of the microgapped IDT (such as shape, gap, width, length) are expected to affect the infrared absorption and the performance of pyroelectric sensor (Fig. 11(b)). Kimata et al. reported the wavelength selective absorption from a plasmonic gratings varying gaps and width [47]. We also currently planned the experiments about structural dependence of IDT on the sensor performance. Therefore, we believe that the large pyroelectric signal obtained was due to the generation of infrared-to-thermal conversion by SPR in the infrared region owing to the microgapped IDT structure and the small amount of charge injection.

Table 1
Comparison of voltage sensitivities of pyroelectric sensors.

Polarization array	In-plane		Out of plane
Film thickness	100 nm		1.3 μm
Device structure	IDT structure (Au electrode)		Sandwich structure (NiCr/VDF/Al)
Poled during annealing	Yes	No	No
Poled after film formation	No	Yes	Yes
Voltage Sensitivity(V W^{-1}), @1 Hz	242	21	72

Finally, Table 1 shows a comparison of the voltage sensitivity of the VDF-based pyroelectric sensor proposed by our group. The voltage sensitivity was obtained based on the division of the output voltage in terms of the infrared incident power and constitutes a general index for the pyroelectric sensor. The microgapped IDT structure fabricated on the SiO_2/Si substrate was 21 V W^{-1} (at 1 Hz) when the polarization was controlled by applying a high electric field after film formation, whereas the sandwich structure fabricated on the Si substrate using Fabry–Perot absorption by NiCr was 72 V W^{-1}. However, the P(VDF/TrFE) thin films with a low electric field applied during the annealing process showed a high value of 242 V W^{-1}. This value is high despite the use of a SiO_2/Si substrate with a high thermal capacity because the temperature change in the element is important for pyroelectric sensors. The temperature change (ΔT) of the P(VDF/TrFE) pyroelectric sensors, which annealed with the low electric fields on the IDT structure on Si substrate, can be roughly estimated to be 3.8 K s^{-1} by using the pyroelectric coefficient (−45 μC m^{-2} K^{-1}) of P(VDF/TrFE), while the ΔT of the sandwiched sensors fabricated on Si substrate is 0.12 K s^{-1}. Thus, the microgapped IDT structure generates an instantaneous ΔT more than 30 times greater than the sandwich structure owing to the SPR phenomenon.

In summary, the high sensitivity obtained in this work can be probably attributed to the low charge injection under the low electric field applied during the annealing process and the enhanced infrared absorption owing to the SPR phenomenon on the IDT structure.

4. Conclusions

The dipoles of P(VDF/TrFE) were oriented between the microgapped IDT structure in the in-plane direction with parallel molecular chain ordering by applying a low electric field during annealing. By applying a low electric field during the annealing process, the molecular chains were induced to the electric field-responsive T_3GT_3G' structure instead

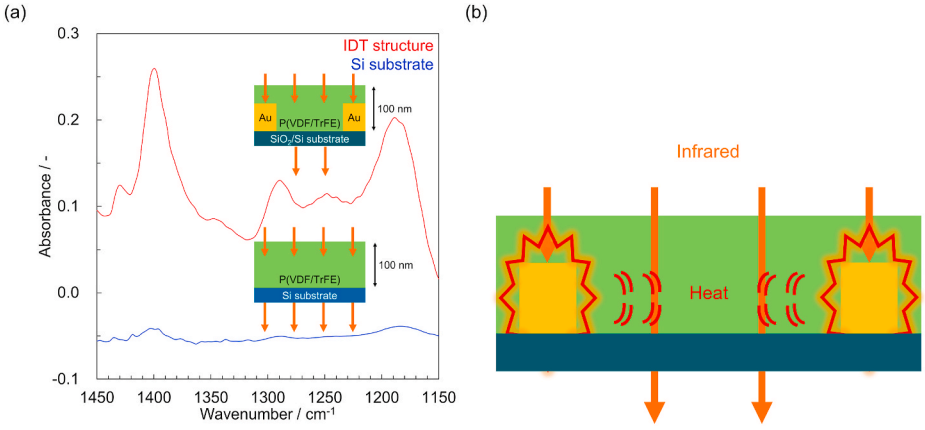

Fig. 11. (a) FT-IR transmission absorption spectra of P(VDF-TrFE) thin films on the microgapped IDT electrodes fabricated on a SiO_2/Si and Si substrate. (b) Infrared-to-thermal conversion model in the IDT structure.

of the *TGTG′* structure, and the rotator phase with T_3GT_3G' structure—similar to the nucleus of the III phase structure—was formed during the cooling process, followed by the transition to the I phase crystalline phase with in-plane dipole alignment. In addition, the application of a low electric field at a temperature above T_{melt}, instead of between $T_{Curie\ 1}$ and T_m, (which is the conventional annealing temperature) was found to be effective. The pyroelectric sensor fabricated by applying a low electric field during the annealing process showed an improved output signal owing to the suppression of charge injection. Moreover, because the sensor can exhibit a high pyroelectric response even though the IDT structure is inherently infrared transmitting, we predict an enhancement in the infrared absorption and improvement in the infrared-to-thermal conversion efficiency using the microgapped IDT structure. Our findings will enable a simple and effective fabrication of highly sensitive SPR-based pyroelectric sensors and allow the exploitation of ferroelectric polymers as new components for non-toxic pyroelectric sensing devices in the future.

Declaration of competing interest

The authors declare that they have no known competing financial interests or personal relationships that could have appeared to influence the work reported in this paper.

Acknowledgment

This work was partly supported by a Grant-in-Aid for Scientific Research from JSPS KAKENHI, CREST from JST, and the Kyoto University Nano Technology Hub in “Nanotechnology Platform Project” sponsored by MEXT, Japan.

References

[1] T. Yoshida, R. Sudo, Application to the air conditioner of the super-resolution thermal sensation sensing technology using the infrared array sensor, J. Jpn. Society of Infrared Science and Technolog 26 (2017) 12.
[2] T. Nomura, Technology trends of automotive sensor, J. Surf. Finish. Soc. Jpn. 67 (2016) 628–632, https://doi.org/10.4139/sfj.67.628.
[3] R. Köhler, N. Neumann, N. Heß, R. Bruchhaus, W. Wersing, M. Simon, Pyroelectric devices based on sputtered PZT thin films, Ferroelectrics 201 (1997) 83–92, https://doi.org/10.1080/00150199708228356.
[4] M. Schreiter, R. Bruchhaus, D. Pitzer, W. Wersing, Sputtering of Self Polarized PZT Films for IR-Detector Arrays, in: Proceedings of the Eleventh I.E.E.E. International Symposium on Applications of Ferroelectrics, 1998, https://doi.org/10.1109/ISAF.1998.786665, 181.
[5] A. Hossain, M.H. Rashid, Pyroelectric detectors and their applications, IEEE Trans. Ind. Appl. 27 (1991) 824–829, https://doi.org/10.1109/28.90335.
[6] S. Vincent, S. Michael, S. Sri, D. Donald, S. Mark, Thin film lithium tantalate (TFLT) pyroelectric detectors, Proc. S.P.I.E. 8261 (2012), 82610q, https://doi.org/10.1117/12.908523. Terahertz Technology and Applications V.
[7] K. Noda, K. Ishida, A. Kubono, T. Horiuchi, H. Yamada, K. Matsushige, Remanent polarization of evaporated films of vinylidene fluoride oligomers, J. Appl. Phys. 93 (2003) 2866–2870, https://doi.org/10.1063/1.1540231.
[8] T. Inoue, A. Mori, Y. Koshiba, M. Misaki, K. Ishida, In-plane polarization switching of highly crystalline vinylidene fluoride oligomer thin films, Appl. Phys. Express 8 (2015), 111601, https://doi.org/10.7567/APEX.8.111601.
[9] K. Noda, K. Ishida, T. Horiuchi, H. Yamada, K. Matsushige, Pyroelectricity of ferroelectric vinylidene fluoride-oligomer-evaporated thin films, Jpn. J. Appl. Phys. 42 (2003) L1334–L1336, https://doi.org/10.1143/JJAP.42.L1334.
[10] Y. Kuroda, Y. Koshiba, M. Misaki, K. Ishida, Y. Ueda, Pyroelectric response of submicron free-standing poly(vinylidene fluoride/trifluoroethylene) copolymer thin films, Appl. Phys. Express 6 (2013), 021601, https://doi.org/10.7567/APEX.6.021601.
[11] R. Hasegawa, M. Kobayashi, H. Tadokoro, Molecular conformation and packing of poly(vinylidene fluoride). stability of three crystalline forms and the effect of high pressure, Polym. J. 3 (1972) 591–599, https://doi.org/10.1295/polymj.3.591.
[12] R. Hasegawa, Y. Takahashi, Y. Chatani, H. Tadokoro, Crystal structures of three crystalline forms of poly(vinylidene fluoride), Polym. J. 3 (1972) 600–610, https://doi.org/10.1295/polymj.3.600.
[13] S.K. Dey, K.D. Budd, D.A. Payne, Thin-film ferroelectrics of PZT of sol–gel processing, I.E.E.E. Trans. Ultrason. Ferroelectr. Freq. Control 35 (1988) 80–81, https://doi.org/10.1109/58.4153.
[14] A. Kobayashi, Y. Koshiba, Y. Ueno, T. Kajihara, Y. Tsujiura, M. Morimoto, S. Horike, T. Fukushima, I. Kanno, K. Ishida, Orientation dependence of power generation on piezoelectric energy harvesting using stretched ferroelectric polymer films, J. Phys.: Conf. Ser. 1052 (2018), 012112, https://doi.org/10.1088/1742-6596/1052/1/012112.
[15] Y. Sutani, T. Fukushima, Y. Koshiba, S. Horike, T. Kodani, T. Kanemura, K. Ishida, Characteristics of an infrared sensor formed with a few molecular layers of vinylidene fluoride oligomers with in situ poling during vacuum evaporation, Jpn. J. Appl. Phys. 59 (2020) SDDF01, https://doi.org/10.7567/1347-4065/ab5502.
[16] J.K. Kim, M.N. Reynolds, S.L. Hsu, Spectroscopic studies on the effect of field strength upon the curie transition of a VDF/TrFE copolymer, J. Polym. Sci. B Polym. Physiol. 31 (1993) 1555–1566, https://doi.org/10.1002/polb.1993.090311112.
[17] J.K. Kim, B.G. Kim, C.L. Vanlencia, J.F. Rabolt, Curie transition, ferroelectric crystal structure, and ferroelectricity of a VDF/TrFE(75/25) copolymer 1. The effect of the consecutive annealing in the ferroelectric state on curie transition and ferroelectric crystal structure, J. Polym. Sci. B Polym. Physiol. 32 (1994) 2435–2444, https://doi.org/10.1002/polb.1994.090321501.
[18] T. Furukawa, Structure and functional properties of ferroelectric polymers, Adv. Colloid Interface Sci. 71–72 (1997) 183–208, https://doi.org/10.1016/S0001-8686(97)90017-8.
[19] Y. Kondo, S. Horike, Y. Koshiba, T. Fukushima, K. Ishida, Directly monitoring and power generation from pulsating 3D heart model with organic flexible piezoelectric device, Jpn. J. Appl. Phys. 59 (2020) SDDF02, https://doi.org/10.7567/1347-4065/ab54f5.
[20] H. Ohigashi, K. Omote, T. Gomyo, Formation of “single crystalline films” of ferroelectric copolymers of vinylidene fluoride and trifluoroethylene, Appl. Phys. Lett. 66 (1995) 3281–3283, https://doi.org/10.1063/1.113730.
[21] T. Tansel, High beta-phase processing of polyvinylidenefluoride for pyroelectric applications, J. Polym. Res. 27 (2020) 95, https://doi.org/10.1007/s10965-020-02073-w.
[22] M. Kobayashi, K. Tashiro, H. Tadokoro, Molecular vibrations of three crystal forms of poly(vinylidene fluoride), Macromolecules 8 (1975) 158–171, https://doi.org/10.1021/ma60044a013.
[23] M.A. Bachmann, W.L. Gordon, J.L. Koenig, J.B. Lando, An infrared study of phase-III poly(vinylidene fluoride), J. Appl. Phys. 50 (1979) 6106–6112, https://doi.org/10.1063/1.325780.
[24] M.A. Bachmann, J.L. Koenig, Vibrational analysis of phase III of poly (vinylidene fluoride), J. Chem. Phys. 74 (1981) 5896–5910, https://doi.org/10.1063/1.440908.
[25] K. Tashiro, Y. Abe, M. Kobayashi, Computer simulation of structure and ferroelectric phase transition of vinylidene fluoride copolymers (1) Vdf content dependence of the crystal structure, Ferroelectrics 171 (1995) 281–297, https://doi.org/10.1080/00150199508018440.
[26] M.N. Reynolds, J.K. Kim, C. Chang, L.S. Hsu, Spectroscopic analysis of the electric field induced structural changes in vinylidene fluoride/trifluoroethylene copolymers, Macromolecules 22 (1988) 1092–1100, https://doi.org/10.1021/ma00193a016.
[27] J.K. Kim, M.N. Reynolds, L.S. Hsu, Spectroscopic analysis of the crystalline and amorphous phases in a vinylidene fluoride/trifluoroethylene copolymer, Macromolecules 22 (1989) 4395–4401, https://doi.org/10.1021/ma00202a001.
[28] K. Tashiro, K. Takano, M. Kobayashi, Y. Chatani, H. Tadokoro, Structure and ferroelectric phase transition of vinylidene fluoride–trifluoroethylene copolymers: 2. VDF 55% copolymer, Polymer 25 (1984) 195–208, https://doi.org/10.1016/0032-3861(84)90326-4.
[29] K. Koga, N. Nakano, T. Hattori, H. Ohigashi, Crystallization, field-induced phase transformation, thermally induced phase transition, and piezoelectric activity in p (vinylidene fluoride-TrFE) copolymers with high molar content of vinylidene fluoride, J. Appl. Phys. 67 (1990) 965–974, https://doi.org/10.1063/1.345706.
[30] H. Ohigashi, T. Hattori, Improvement of piezoelectric properties of poly(vinylidene fluoride) and its copolymers by crystallization under high pressures, Ferroelectrics 171 (1995) 11–32, https://doi.org/10.1080/00150199508018419.
[31] T. Yamada, D. Ito, T. Sluka, O. Sakata, H. Tanaka, H. Funakubo, T. Namazu, N. Wakiya, M. Yoshino, T. Nagasaki, N. Setter, Charge screening strategy for domain pattern control in nano-scale ferroelectric systems, Sci. Rep. 7 (2017) 5236, https://doi.org/10.1038/s41598-017-05475-x.
[32] C. Fabry, A. Perot, Théorie et applications d’une nouvelle méthode de spectroscopie interférentielle, Ann. de Chim. et de Phys. 16 (1899) 115–144.
[33] S.W. Mcknight, K.P. Stewart, H.D. Drew, K. Moorjani, Wavelength-independent anti-interference coating for the far-infrared, Infrared Phys. 27 (1987) 327–333, https://doi.org/10.1016/0020-0891(87)90074-1.
[34] D. Lienhard, F. Heepmann, B. Ploss, Thin nickel films as absorbers in pyroelectric sensor arrays, Microelectron. Eng. 29 (1995) 101–104, https://doi.org/10.1016/0167-9317(95)00124-7.
[35] S. Bauer, S. Bauer-Gogonea, B. Ploss, The physics of pyroelectric infrared devices, Appl. Phys. B 54 (1992) 544–551, https://doi.org/10.1007/BF00325524.
[36] S. Bauer, S. Bauer-Gogonea, W. Becker, R. Fettig, B. Ploss, W. Ruppel, W. von Münch, Thin metal films as absorbers for infrared sensors, Sens. Actuators, A 37–38 (1993) 497–501, https://doi.org/10.1016/0924-4247(93)80085-U.
[37] A.D. Parsons, D.J. Pedder, Thin-film infrared absorber structures for advanced thermal detectors, J. Vac. Sci. Technol. A 6 (1988) 1686–1689, https://doi.org/10.1116/1.575308.
[38] L. Zhang, T. Yang, X. Wu, X. Yao, Preparation and behavior of infrared focal plane linear array using composite ferroelectric film, Ceram. Int. 30 (2004) 1851–1855, https://doi.org/10.1016/j.ceramint.2003.12.056.
[39] A. Hartstein, J.R. Kirtley, J.C. Tsang, Enhancement of the infrared absorption from molecular monolayers with thin metal overlayers, Phys. Rev. Lett. 45 (1980) 201–204, https://doi.org/10.1103/PhysRevLett.45.201.

[40] M. Osawa, Dynamic processes in electrochemical reactions studied by surface-enhanced infrared absorption spectroscopy (SEIRAS), Bull. Chem. Soc. Jpn. 70 (1997) 2861–2880, https://doi.org/10.1246/bcsj.70.2861.
[41] M. Fleischmann, P.J. Hendra, A.J. Mcquillan, Raman spectra of pyridine adsorbed at a silver electrode, Chem. Phys. Lett. 26 (1974) 163–166, https://doi.org/10.1016/0009-2614(74)85388-1.
[42] T.W. Ebbesen, H.J. Lezec, H.F. Ghaemi, T. Thio, P.A. Wolff, Extraordinary optical transmission through sub-wavelength hole arrays, Nature 391 (1998) 667–669, https://doi.org/10.1038/35570.
[43] H. Liu, P. Lalanne, Microscopic theory of the extraordinary optical transmission, Nature 452 (2008) 728–731, https://doi.org/10.1038/nature06762.
[44] S. Ogawa, K. Okada, N. Fukushima, M. Kimata, Wavelength selective uncooled infrared sensor by plasmonics, Appl. Phys. Lett. 100 (2012), 021111, https://doi.org/10.1063/1.3673856.
[45] S. Ogawa, M. Kimata, Metal-insulator-metal-based plasmonic metamaterial absorbers at visible and infrared wavelengths: a review, Materials 11 (2018) 458, https://doi.org/10.3390/ma11030458.
[46] T.D. Dao, S. Ishii, A.T. Doan, Y. Wada, A. Ohi, T. Nabatame, T. Nagao, An on-chip quad-wavelength pyroelectric sensor for spectroscopic infrared sensing, Adv. Sci. 6 (2019), 1900579, https://doi.org/10.1002/advs.201900579.
[47] S. Ogawa, M. Kimata, Direct fabrication and characterization of high-aspect-ratio plasmonic nanogratings using tapered-sidewall molds, Opt. Mater. Express 7 (2017) 633, https://doi.org/10.1364/OME.7.000633.